Electron Bremsstrahlung Hard X-Ray Spectra, Electron Distributions and Energetics in the 2002 July 23 Solar Flare

Gordon D. Holman, Linhui Sui[1], and Richard A. Schwartz[2]

Laboratory for Astronomy and Solar Physics, Code 682, NASA/Goddard Space Flight Center, Greenbelt, MD 20771

holman@stars.gsfc.nasa.gov, lhsui@stars.gsfc.nasa.gov, richard.schwartz@gsfc.nasa.gov

and

A. Gordon Emslie

Department of Physics, The University of Alabama in Huntsville, Huntsville, AL 35899

emslieg@uah.edu

ABSTRACT

We present and analyze the first high-resolution hard X-ray spectra from a solar flare observed in both X-ray/γ-ray continuum and γ-ray lines. The 2002 July 23 flare was observed by the Ramaty High Energy Solar Spectroscopic Imager (RHESSI). The spatially integrated photon flux spectra are well fitted by a double power law during the rise of the flare, and by the combination of an isothermal component and a double power law after the initial rise phase. The flare plasma temperature peaks at 40 MK around the time of peak hard X-ray emission and remains above 20 MK over 30 min later. We derive the evolution of the nonthermal electron density distribution by directly fitting the RHESSI X-ray spectra with the thick-target bremsstrahlung from a double power-law electron distribution. We also derive the evolution of the mean electron flux, which does not assume thick-target emission. We find that the injected nonthermal electrons are well described by a double power-law distribution throughout the flare. We compare the energy content of the thermal flare plasma observed by RHESSI and GOES with the energy contained in the nonthermal electrons. We find that

[1]The Catholic University of America

[2]SSAI

the total energy deposited into the flare plasma by nonthermal electrons during the rise phase of the flare is equal to or greater than the energy in the thermal plasma observed by GOES and RHESSI.

Subject headings: Sun: flares, Sun: X-rays, gamma rays

1. Introduction

Since its launch on 2002 February 5, the Ramaty High Energy Solar Spectroscopic Imager (RHESSI) has been obtaining unprecedented images and spectra of solar flares in hard X-rays and γ-rays (see Lin et al. 2000 for a description of the RHESSI instrument and its capabilities). The hard X-ray/γ-ray continuum traces energetic electrons accelerated in flares, while γ-ray lines trace accelerated ions (e.g., Hudson & Ryan 1995). The first (and, currently, the only) γ-ray line flare observed by RHESSI occurred on 2002 July 23. This observation provides a rare opportunity to compare electron and ion acceleration in a single flare.

This Letter focuses on electrons in the July 23 flare. Spatially integrated photon flux spectra are derived from the RHESSI data in the 10 keV – 300 keV energy range. These spectra are fitted with computations of the bremsstrahlung flux from model electron distribution functions to deduce the temporal evolution of the flare electrons. Hard X-ray images and imaged spectra are obtained and analyzed in Krucker et al. (2003) and Emslie et al. (2003), respectively. The flare γ-ray bremsstrahlung above 300 keV is discussed in Share et al. (2003). A comprehensive summary of the flare observations and their implications is presented in Lin et al. (2003).

We obtain the hard X-ray spectra and their time evolution in Section 2. In Section 3 we derive mean electron flux distributions (Brown, Emslie & Kontar 2003) from the RHESSI spectra. These distributions are independent of the thick-target assumption and, therefore, are well suited for comparison with electron distributions computed from theoretical flare models. Our mean electron distributions, obtained through forward fitting, are compared with mean electron flux distributions obtained through direct inversion in Piana et al. (2003). In Section 4, assuming that the emission is thick-target bremsstrahlung, we obtain the evolution of the electron density distribution. We use these density distributions to compute the electron energy flux and its time evolution, and the total energy in accelerated electrons. These are compared to the evolution of the energy content of the thermal plasma observed by RHESSI and GOES. Our results are discussed in Section 5.

2. X-Ray Spectra

The time history of the flare emission in three energy bands is shown in Figure 1a. RHESSI uses two attenuators, a thin aluminum shutter and a thick aluminum shutter, to avoid saturating the detectors during large flares. The July 23 flare was observed in two attenuator states. The instrument was primarily in the A3 state, with both attenuators in place. Early in the flare before 00:26:08 UT and late in the flare after 00:59:21 UT the instrument was in the A1 state, with only the thin attenuator in place. There were also four brief periods during which the instrument switched from A3 to A1 and back to A3. These transitions in attenuator state are apparent in the time history of the lowest energy band in Fig. 1a. The flux calibration is currently uncertain during the four brief transition periods. These time periods appear as gaps in subsequent results derived from the data.

Spectral fits were obtained using the Solar Software Tree (SSW) spectral analysis routine (SPEX, see Schwartz 1996, Smith et al. 2003). Before fitting the data, we corrected the observed counts for pulse pileup and decimation. Background counts were subtracted from the data by obtaining a linear fit through the background levels before and after the flare. Because the attenuators substantially diminish the photon flux that reaches the RHESSI detectors at low energies, spectra obtained in the A1 state were fitted down to 10 keV photon energies while spectra obtained in the A3 state were fitted down to 15 keV. The spectra were fitted up to 300 keV unless a contribution from background counts was significant below this energy. At times earlier than 00:26:00 UT, for example, spectral fits could not be obtained above 60 keV. For photon fluxes well above the background, we estimate the uncertainty in the fluxes to be 2%. The absolute uncertainty in the RHESSI fluxes is currently not known. This estimate was obtained by requiring the normalized χ^2 for our spectral fits to be on the order of one (rather than much less than one).

The count spectra in each 20-s time interval were fitted with the combination of an isothermal bremsstrahlung spectrum and a double-power-law photon spectrum. This provides six fit parameters: the temperature (T) and emission measure (EM) of the isothermal component, lower (γ_L) and upper (γ_U) spectral indices and the energy at which the spectral break occurs (E_B), and the normalization for the double-power-law spectrum, taken to be the photon flux at 50 keV (F_{50}). We find that the spectra during the early rise of the flare are best fit by a double power law alone. Late in the flare, only the isothermal component is evident.

The time history of the temperature of the isothermal component is shown in Fig. 1b (plus signs). The temperature rapidly rises to "superhot" values (Lin et al. 1981) as high as 40 MK. This hot thermal emission is consistent with the spectrum of the "coronal" source observed in RHESSI images (Emslie et al. 2003). The plasma gradually cools after the end of

the first peak in the flare emission, with some reheating in subsequent peaks. Temperatures derived from GOES data are shown for comparison (solid curve). Throughout the flare the temperatures derived from the RHESSI data are typically around 10 MK higher than those derived from the GOES data. Thirty-seven minutes after reaching its peak value of 40 MK, the plasma temperature derived from the RHESSI spectra remains above 20 MK.

The emission measure of the isothermal component is plotted in Fig. 1c (plus signs). Although the peak temperature is similar to that obtained by Lin et al. (1981) for the 1980 June 27 flare, the peak emission measure is thirty times greater. The GOES emission measure (solid curve, scaled by a factor of 0.25) always exceeds the RHESSI emission measure, as expected for lower temperature plasma.

The spectral indices γ_L and γ_U, defined by Flux $\propto E^{-\gamma}$, have values between 2.5 and 3.5 throughout most of the flare (Fig. 1d). These spectral indices and their time evolution are consistent with the spectra obtained for the "footpoint" sources observed in RHESSI images (Emslie et al. 2003). Earlier in the flare, before the impulsive rise, the spectral indices are much greater, on the order of 5 to 7. While $\Delta\gamma$ is on the order of one before the impulsive rise, it is subsequently on the order of 0.5 or less. When the nonthermal spectrum is observable after 00:40:00 UT, it is best fit with a single power law. The break energy, plotted in Fig. 1e, increases from values below 50 keV before the impulsive rise of the flare to values in the range 70–125 keV.

Fig. 1f shows the time history of the photon flux at 50 keV. This closely follows the 40–100 keV light curve.

3. Mean Electron Flux Distributions

The mean electron flux is the spatially averaged value of the electron flux weighted by the plasma density (Brown et al. 2003). Deducing the mean electron flux from a photon spectrum is equivalent to deducing the electron flux under the assumption that the radiation is thin-target bremsstrahlung. In this paper we compute the mean electron flux in forty consecutive 20 s time intervals near the peak of the flare. We do this by assuming that the functional form of the mean electron flux is a double power law and then obtaining best fits to the bremsstrahlung spectra computed from this distribution. The results are shown in Figure 2. For these and subsequent computations in Section 4, the bremsstrahlung cross section of Haug (1997) is used with the Elwert (1939) correction.

As expected for thin-target bremsstrahlung, the power-law indices for the mean electron flux distribution (Fig. 2b) are smaller than the photon spectral indices (Fig. 1d) by about

1. The break energies for the electron distributions (Fig. 2c) are higher than those for the photon spectra (Fig. 1e) because the photons are produced by electrons with higher energies than the photon energy. The bremsstrahlung spectrum only begins to flatten at energies immediately below the break in the electron distribution. The normalization in Fig. 2d is $\overline{n}V\overline{F}_{10}$, where V is the volume of the emitting region, $\overline{n}$ is the mean density in the emitting volume, and $\overline{F}_{10}$ is the mean electron flux distribution integrated from 10 keV to the highest electron energy in the distribution.

The spectral fit for the interval 00:30:00–00:30:20 UT is shown in the top panel of Figure 3. The residuals from this fit, defined as $(F_{obs}(E) - F_{fit}(E))/\sigma(E)$, where E is the photon energy, F_{obs} is the observed photon flux, F_{fit} is the photon flux given by the model at energy E, and σ is the uncertainty in the observed flux, are plotted in the bottom panel. The residuals are limited to about the $\pm 2\sigma$ level, but they are not entirely random. The systematic deviation below 20 keV may be due to our currently uncertain knowledge of the steep RHESSI response function at low energies when both attenuators are in place, or to the contribution of lower temperature plasma to the thermal bremsstrahlung. An inaccurate background subtraction could explain any systematic trend above 200 keV. Of particular physical interest is the oscillation between 20 keV and 50 keV. This may indicate that our correction for pulse pileup is not entirely correct. On the other hand, this oscillation might be associated with X-ray photons Compton scattered in the photosphere (albedo) or partial ionization in the interaction region. These possibilities are considered by Alexander & Brown (2003) and Kontar et al. (2003), respectively.

Piana et al. (2003) derive mean electron flux distributions from this flare data using a direct inversion technique. Their results are quite different from the double power-law distributions obtained here, showing considerably more structure in the electron distributions. Both distributions provide a good fit to the photon spectra. The differences in these derived electron distributions highlight the fact that there is generally not a unique electron distribution associated with an observed photon spectrum. Nevertheless, the spectral fits can rule out many models, and RHESSI's combination of high spectral and spatial resolution allows us to test physical processses and models that could not be adequately addressed with previous observations.

4. Electron Density Distributions and Energetics

Electron density distributions are computed assuming that the emission is thick-target bremsstrahlung (Brown 1971) and that the electron distribution is a double power law. The thick-target bremsstrahlung from this electron distribution is numerically computed and best

fits to the RHESSI spectra are obtained. The results are shown in Figure 4. Note that the electron flux distribution can be derived from the density distribution by multiplying the density distribution by the electron speed.

The upper power-law indices (triangles, Fig. 4b) are larger by about 1.5 than the upper photon spectral indices, as expected ($\delta_U \simeq \gamma_U + 1.5$). The lower power-law indices are only steeper by about 1, however, because fewer electrons are present above the break energy than would have been present for a single power law. The upper power-law index throughout much of the flare of about 4.5 is consistent with the value estimated from radio observations (White et al. 2003). The break energy (Fig. 4c) increases with time from values around 30 keV to values in excess of 300 keV. The distributions before 00:26:00 UT are also consistent with a single power law and a high energy cutoff in the electron distribution that increases from 40 keV at early times to as high as 100 keV at later times. We found that these spectra could not be adequately fit with a low-energy cutoff or an isothermal distribution, however.

The normalization for the double power-law electron density distribution plotted in Fig. 4d is the total density of nonthermal electrons above 10 keV (n_{10}) times the area of the thick-target interaction region (A). For an area of 10^{19} cm^2, on the order of that shown by the RHESSI image at 00:25:40 UT (see Krucker et al. 2003), this gives a peak density in suprathermal electrons above 10 keV of 3×10^9 cm^{-3}. Later in the flare the observed nonthermal source area is as low as 10^{17} cm^2, giving even higher values of n_{10}. At these times, however, because of the presence of the hot thermal component, the low-energy cutoff in the electron distribution may be as high as 30 or 40 keV, giving a smaller value for the actual density. Nevertheless, the nonthermal electron density becomes quite high in this flare. The radio observations also indicate a high density of nonthermal electrons (White et al. 2003).

The total accumulated energy deposited into the flare plasma by electrons with energies above 10 keV is plotted as a function of time in Fig. 4e (dotted curve). This is obtained by integrating the electron flux distribution derived for each 20 s interval, $n(E)vA$, over all energies above 10 keV, multiplying by the time interval (20 s) and obtaining the sum of these energies up to the time of interest. Most of this energy is deposited before 00:26:00 UT, although there is additional energy input after this time. The total energy injected by these electrons is found to be 4×10^{32} erg.

The energy contained in the thermal plasmas observed by RHESSI (dot-dash line) and by GOES (solid line) is also plotted in Fig. 4e, assuming a plasma density of 1×10^{10} cm^{-3}. From the temperature and emission measure derived from the observations, we are able to compute the product of the plasma density and energy, $n(3nkTV)$. The energy is higher for a plasma density smaller than 10^{10} cm^{-3}, and lower for a density greater than 10^{10} cm^{-3}.

We see from Fig. 1e that the energy in >10 keV electrons exceeds the energy in the plasma observed by both RHESSI and GOES. The energy in the plasma is not likely to be higher than the plotted values because, using the emission measure from Fig. 1c, the plasma volume with a density of 10^{10} cm^{-3} is already quite large: 9×10^{29} cm^3. The RHESSI images (see Krucker et al. 2003) do not indicate such a large flare volume. A higher plasma energy and lower density would require an even larger volume.

Since 10 keV is just an instrumentally determined cutoff energy, the energy deposited by the nonthermal electrons may be even greater. Emslie (2003) shows how the temperature of the target plasma limits the energy that can be deposited into the plasma. The energy injected into the plasma is significantly less than the electron energy computed above a low-energy cutoff if the cutoff energy is less than $5kT$, where T is the temperature of the target plasma. Before 00:26:00 UT there is no evidence for plasma temperatures above 20 MK, or $kT = 1.7$ keV. Therefore, the computed injection energies before this time are accurate. Using the results of Emslie, we can compute the maximum energy these electrons might have injected into the flare plasma. We find this to be 9×10^{34} erg, well above the maximum total energy that has been deduced previously for even the largest solar flares. If the temperature of the target plasma was as high as the temperatures deduced from the RHESSI spectra after 00:26:00 UT, we have overestimated the energy injected into the plasma at these times. Instead of increasing to 4×10^{32} erg, the curve in Fig. 4e remains flat at about 3×10^{32} erg.

Our result for the energy injected by nonthermal electrons depends on our nonthermal interpretation of the double power-law fits before 00:26:00 UT. In view of the significance of this result, we are exploring multithermal and other more complex models for this period. We note, however, that a multithermal fit will require higher temperatures and, at the lower contributing temperatures, higher emission measures. It is also not apparent how the multithermal spectrum can logically evolve into the flatter power-law spectra and 30–40 MK thermal component present during the impulsive phase of the flare. The combination of RHESSI's spectra and images may reveal the most likely scenario for this early phase of the flare.

5. Conclusions

The RHESSI spectra presented and analyzed here are the most detailed hard X-ray spectra ever obtained for a large flare. Although these spectra are well fitted by isothermal (exponential) and double power-law photon distributions, fitting these spectra with the bremsstrahlung computed from model electron distributions is an important part of the analysis of these spectra. The electron distributions allow a more physical interpretation

of the data and smooth out the unphysically sharp break in the double power-law photon spectrum. Even fits with a double power-law electron distribution, however, show systematic residuals at the level of a few percent, as in Fig. 3b. Understanding these residuals will also be an important part of the analysis of RHESSI spectra.

The July 23 flare hard X-ray spectral data provide strong support for the longstanding impression that the energy in accelerated electrons is a major part of the energy released in many if not all flares. Unless radiation from a multi-thermal plasma contributes substantially to the spectra before 00:26:00 UT, which does not appear to be supported by the shape and evolution of these spectra, the total energy injected by nonthermal electrons exceeds the energy content of at least the hot thermal plasma observed by RHESSI and by GOES. The evolution of the energy contained in nonthermal electrons later in the flare merits a careful comparison with the evolution of the energy in the thermal plasma, but this energy is relatively small compared to that injected before 00:26:00 UT.

The information extracted from these spatially integrated spectra can only be fully appreciated and understood through comparison with RHESSI images and imaged spectra, and with related observations of the flare. A synthesis and discussion of the overall flare data is contained in Lin et al. (2003).

This work was supported in part by the RHESSI Project and the NASA Sun-Earth Connection program. We thank Sally House for translating the bremsstrahlung codes from Fortran into IDL, and Paul Bilodeau for his help with the SPEX software and with integrating the bremsstrahlung codes with the SPEX software. We thank Brian Dennis for his comments on the manuscript. This work would not have been possible without the dedicated efforts of the entire RHESSI team.

REFERENCES

Alexander, R. C. & Brown, J. C. 2002, Sol. Phys., in press

Brown, J. C. 1971, Sol. Phys., 18, 489

Brown, J. C., Emslie, A. G. & Kontar, E. P. 2003, ApJ, this issue

Elwert, G. 1939, Ann. Physik, 34, 178

Emslie, A. G. 2003, ApJ, this issue

Emslie, A. G., Kontar, E. P., Krucker, S. & Lin, R. P. 2003, ApJ, this issue

Haug, E. 1997, A&A, 326, 417

Hudson, H. & Ryan, J. 1995, ARA&A, 33, 239

Kontar, E. P., Emslie, A. G., Krucker, S. & Lin, R. P. 2003, ApJ, this issue

Krucker, S., Hurford, G. J. & Lin, R. P. 2003, ApJ, this issue

Lin, R. P., Schwartz, R. A., Pelling, R. M. & Hurley, K. C. 1981, ApJ, 251, L109

Lin, R. P., & the HESSI Team. 2000, in ASP Conf. Ser. 206, High Energy Solar Physics – Anticipating HESSI, ed. Ramaty, R., & Mandzhavidze, N. (San Francisco: ASP), 1

Lin, R. P., et al. 2003, ApJ, this issue

Piana, M., Massone, A., A. G., Kontar, Emslie, E. P., Brown, J. C. & Schwartz, R. A. 2003, ApJ, this issue

Schwartz, R. A. 1996, "Compton Gamma Ray Observatory Phase 4 Guest Investigator Program: Solar Flare Hard X-ray Spectroscopy," Technical Report, NASA Goddard Space Flight Center

Share, G., Murphy, R. J., Lin, R. P., Smith, D. M. & Schwartz, R. A. 2003, ApJ, this issue

Smith, D., et al. 2002, Sol. Phys., in press

White, S. M., Krucker, S., Shibasaki, K., Yokoyama, T., Shimojo, M. & Kundu, M. R. 2003, ApJ, this issue

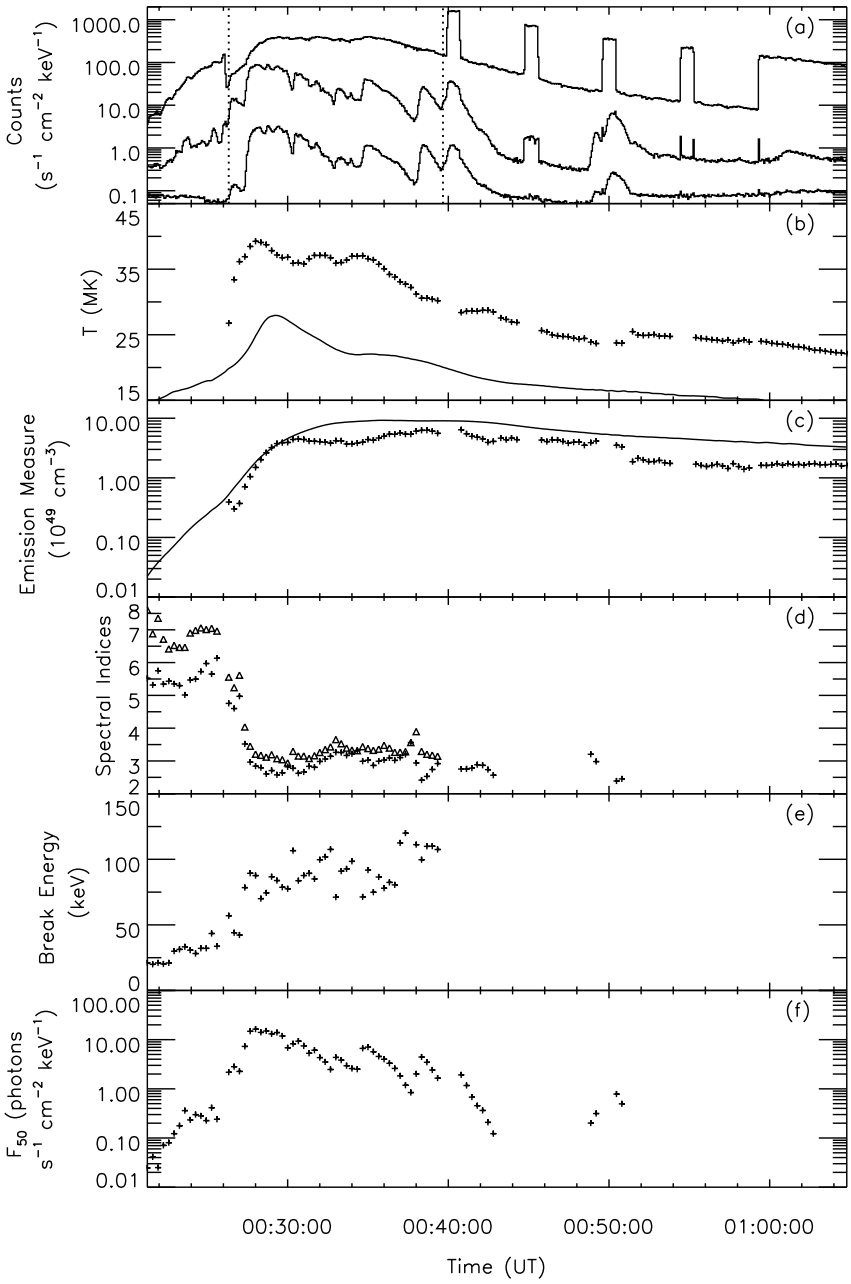

Fig. 1.— RHESSI X-ray light curves and time history of fit parameters. (a) Light curves in three energy bands, scaled to avoid overlap. The energy bands and scale factors are 12–40 keV (top curve, ×0.6), 40–100 keV (middle curve, ×3), and 100–300 keV (bottom curve, ×1). The dotted vertical lines show the start time and the end time for the results of Fig. 2. (b) Time history of the temperature of the isothermal component (20 s time resolution, plus signs). The solid curve is the temperature derived from GOES data. (c) Time history of the isothermal emission measure (plus signs). The solid curve is the emission measure derived from GOES data, scaled by a factor of 0.25. (d) Time history of the double power-law spectral indices (spectral index below break, plus signs; spectral index above break, triangles). (e) Time history of the break energy in the double power-law spectra. (f) Time history of the photon flux at 50 keV, determined from the double power-law fit.

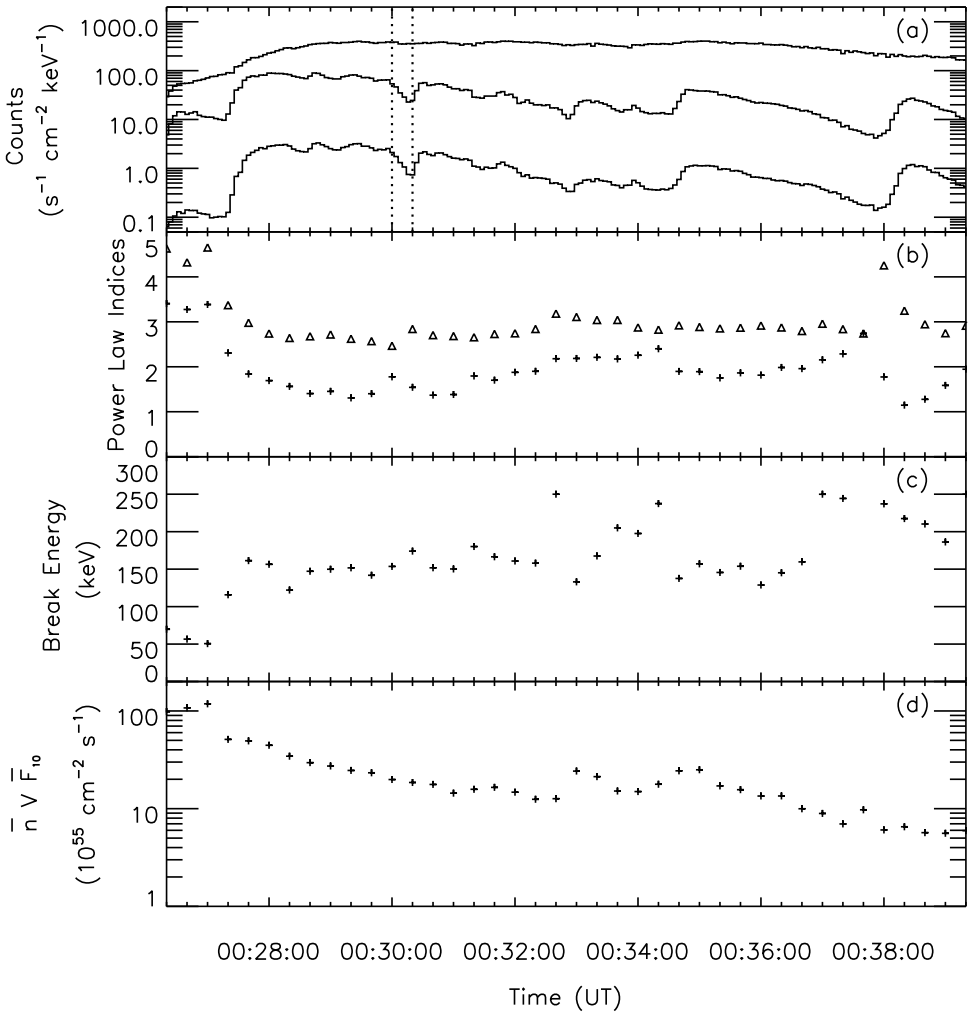

Fig. 2.— Time history of mean electron flux fit parameters. (a) Light curves in three energy bands (same bands and scale factors as Fig. 1a). The dotted vertical lines show the beginning and end of the integration time interval for the spectrum in Fig. 3. (b) Time history of the upper and lower power-law indices (20 s time resolution, same symbols as Fig. 1d) (c) Time history of the break energy in the double power-law mean electron flux distribution. (d) Normalization of the mean electron flux distribution (see text).

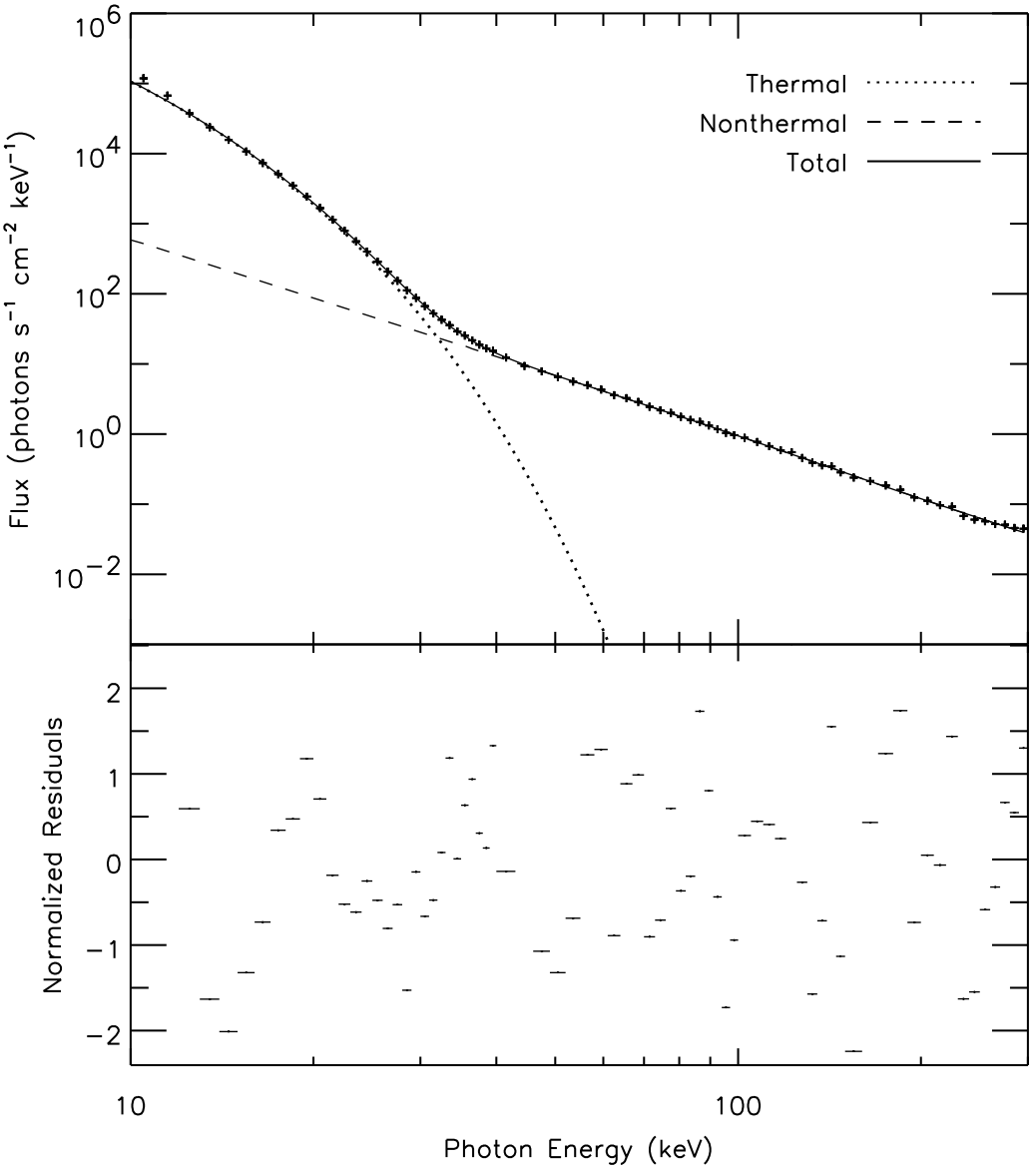

Fig. 3.— Fit and residuals for the 00:30:00–00:30:20 UT time interval. The fit in the upper panel is the bremsstrahlung from an isothermal plasma (dotted curve) and a double power-law mean electron flux distribution (dashed curve). The solid curve is the total fit. The best fit parameters were $EM = 3.9 \times 10^{49}$ cm^{-3}, $T = 37$ MK, $\overline{n}V\overline{F}_{10} = 2 \times 10^{56}$ cm^{-2} s^{-1}, $\delta_L = 1.8$, $E_B = 154$ keV, and $\delta_U = 2.5$ with a normalized χ^2 of 1.2. The data points are represented by plus signs. The residuals in the bottom panel are defined as the observed flux minus the model flux divided by sigma, where sigma is the estimated one sigma error in each data point.

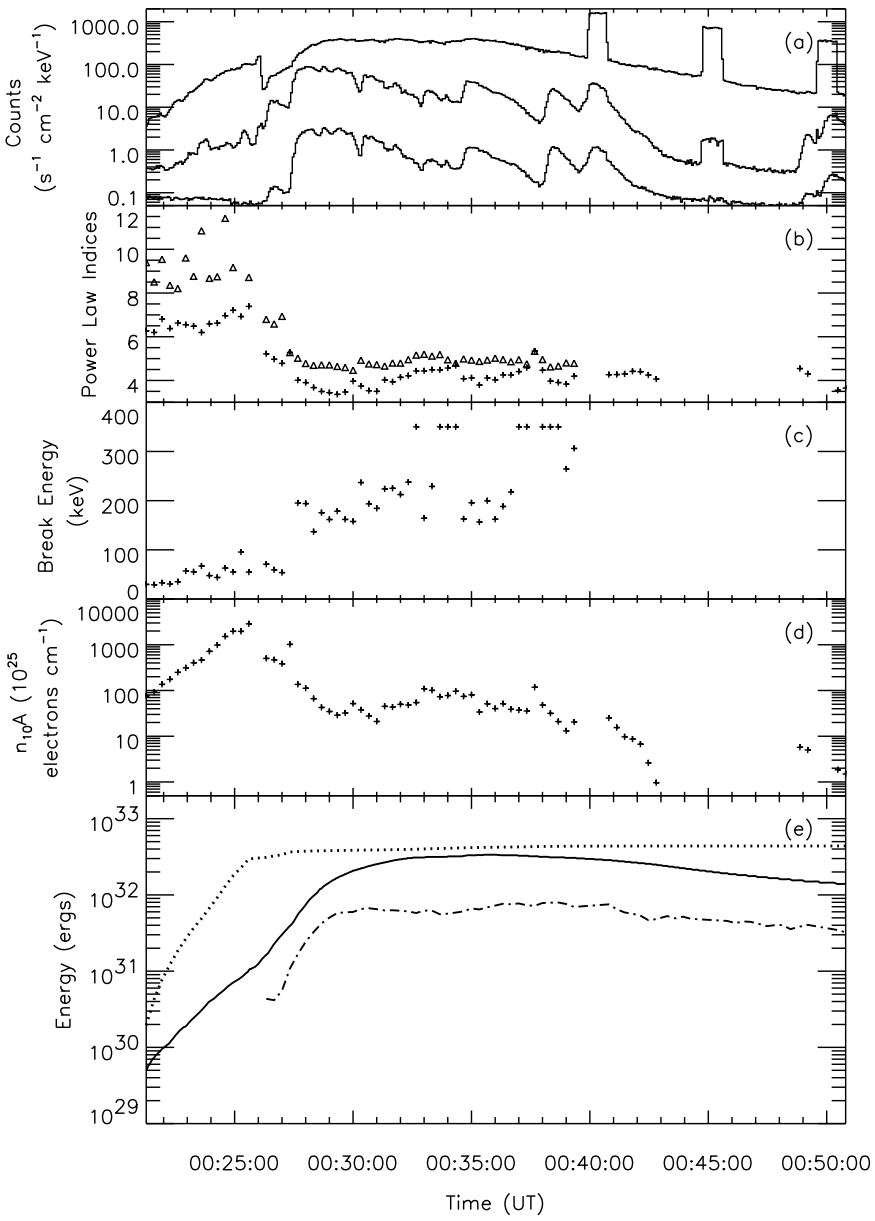

Fig. 4.— Thick-target bremsstrahlung electron density distribution fit parameters and energetics. (a) X-ray light curves in three energy bands (see Fig. 1a). (b) Time history of the upper and lower power-law indices (20 s time resolution, same symbols as Fig. 1d) (c) Time history of the break energy in the double power-law electron density distribution. (d) Normalization of the nonthermal electron density distribution (see text). (e) Thermal and nonthermal energetics. The time history of the energy in the GOES (solid line) and RHESSI (dashed line) isothermal fits is plotted assuming a constant plasma density of 10^{10} cm^{-3}. This is compared to the accumulated energy in nonthermal electrons with energies above 10 keV (dotted curve, see text).